Hindawi
Shock and Vibration
Volume 2018, Article ID 8067416, 13 pages
https://doi.org/10.1155/2018/8067416

Research Article

Optimal SES Selection Based on SVD and Its Application to Incipient Bearing Fault Diagnosis

Longlong Li, Yahui Cui, Runlin Chen, and Xiaolin Liu

School of Mechanical and Precision Instrument Engineering, Xi'an University of Technology, Xi'an, China

Correspondence should be addressed to Longlong Li; longlongli@stu.xaut.edu.cn

Received 12 July 2018; Revised 29 October 2018; Accepted 14 November 2018; Published 2 December 2018

Academic Editor: Mahdi Mohammadpour

Rotating machinery has extensive industrial applications, and rolling element bearing (REB) is one of the core parts. To distinguish the incipient fault of bearing before it steps into serious failure is the main task of condition monitoring and fault diagnosis technology which could guarantee the reliability and security of rotating machinery. The early defect occurring in the REB is too weak and manifests itself in heavy surrounding noise, thus leading to the inefficiency of the fault detection techniques. Aiming at the vibration signal purification and promoting the potential of defects detection, a new method is proposed in this paper based on the combination of singular value decomposition (SVD) technique and squared envelope spectrum (SES). The kurtosis of SES (KSES) is employed to select the optimal singular component (SC) obtained by applying SVD to vibration signal, which provides the information of the REB for fault diagnosis. Moreover, the rolling bearing accelerated life test with the bearing running from normal state to failure is adopted to evaluate the performance of the SVD-KSES, and results demonstrate the proposed approach can detect the incipient faults from vibration signal in the natural degradation process.

1. Introduction

Rotating machinery has various applications in modern industries such as wind power, marine, and helicopter among which rolling element bearing is one of the most commonly used components to support the rotating parts. Unfortunately, according to the surveys conducted by the electric power research institute, the REB-related faults account for 40% failures in induction motors [1] and 64% of gearbox failures [2]. The occurrence of any REB defects, as well as the performance deterioration, affects the working performance of other parts and thus causing a deficiency of the entire machine, unscheduled shutdowns, economic loss, and even industrial casualties [3]. Therefore, it becomes significant to implement effective techniques to monitor the condition of bearings. The in-time failure detection of bearing can ensure the reliability and security of the machinery and personnel security as well.

There are several data acquisition techniques commonly applied to get health information about the working state of bearing such as acoustic measurement, temperature monitoring, oil debris analysis, and vibration monitoring. In addition, the vibration-signal-based techniques are extensively adopted in the industry for kinds of rotating equipment since they contain most information and are proven to be an efficient tool for bearing fault diagnosis [4]. The vibration signal can be obtained through the bearing housing or cast at a low cost, which makes the vibration-based fault diagnosis techniques more popular. A fault vibration signal of REB is assumed to be a series of impulses with quasiperiodic damping components, which is also overwhelmed by surrounding noises and contaminated due to rotating speed [5], gear noises, etc. These impulses are generated due to the passing of rolling elements over the defected zone. During the early stage of fault development, the background vibration and noise are so strong and bury the fault-related impulses, which makes it difficult to carry out vibration-signal-based fault diagnosis. Therefore, reliable signal processing methods are under high demand to extract and distinguish the fault features manifested in the raw signals with high accuracy promptly.

Various studies have implemented diagnosis algorithms using advanced signal processing techniques to enhance diagnostic performance. For machinery fault diagnosis based on

vibration, there are two main steps, i.e., feature extraction and pattern recognition. With respect to REB vibration signals, plenty of methods based on time domain, frequency domain, or time-frequency analysis are proposed such as envelope analysis [6], spectral kurtosis [7], wavelet transform [8], empirical mode decomposition [9], and Hilbert-Huang transform [10].

The SVD method has promising application in signal processing and has been extensively used in many modern fields such as image processing, noise elimination [11], sensor anomaly detection, and fault-related feature extraction [11–13]. The singular values (SVs) are commonly used to form characteristic feature vector based on which the fault identification can be realized [12, 13]. By applying SVD to the instantaneous amplitude matrices, which is obtained by using Hilbert-Huang transform (HHT) to rolling bearing signals, singular value vectors were considered as the fault features [10]. Moreover, singular spectrum analysis (SSA), derived from SVD, is a nonparametric technique of time series analysis which is based on multivariate statistics and decomposes a signal into several independent components whose sum gives the origin signal [14]. Muruganatham et al. [15] decomposed the acquired vibration signals into an additive set of principal components by implementing SSA and the SVs of the selected number taken as fault features, which were fed to artificial neural network for the purpose of automated fault diagnosis. Quaternion singular spectrum analysis (QSSA), improved by using convex optimization, was proposed to analyze multidimensional channel signals, and in addition, artificial signal as well as the public dataset verified the effectiveness of the QSSA [16]. Additionally, performance evaluation of feature extraction of SSA for ball bearing vibration signals has been done where the singular value ratio (SVR) spectrum was introduced to make a good local identification on the periodic component [17]. To the best of the authors' knowledge, SVs and SVR in these literatures were based on signal energy which may tend to emphasize the high energy regular components while ignoring faint feature induced by early fault [18]. In addition, the effect of each single SC to the accumulative SC is less considered but worth of a trial, which is the very issue of our scheme and evaluated by kurtosis of SES amplitudes from frequency domain. In summary, vibration signal can be decomposed into a set of SCs for further analysis in REB fault diagnosis.

Due to the fast computation efficiency and excellent performance to indicate impulsiveness in the vibration signal, kurtosis is commonly regarded as an object function for fault diagnosis [19]. Moreover, kurtosis-based indexes have been employed to enhance the available techniques in rolling fault diagnosis, such as spectral kurtosis [20, 21], kurtogram [22], and protrugram [23]. The protrugram method, proposed by Barszcz and JabŁoński [23], utilizes kurtosis of envelope spectrum amplitudes to describe the cyclostationarity and further selects optimal resonant frequency band as well as to detect transient impulses with vibration signal in low signal-to-noise ratios. Antoni [24] proposed the SE infogram and SES infogram based on the negentropy of the squared envelope and the SES, respectively. Besides, most of the available diagnosis approaches of REB present the fault characteristic frequency by the envelope spectrum, and kurtosis of SES can reflect the spectrum potential to convey fault information which is on the basis that kurtosis value increases when obvious fault characteristic frequency (FCF) and its harmonics emerge in spectrum. In other words, kurtosis value of SES is big if the apparent FCF can be observed in envelope spectrum. Motivated by thoughts of protrugram and SE, SES infogram, the kurtosis of squared envelope spectrum amplitudes, is employed to evaluate the effect of each SC to the final one, which is expected to extract incipient fault from REB vibration signal.

Based on the above introduction, a new scheme named SVD-KSES, selecting the optimal SC during the SVD process based on kurtosis of squared envelope spectrum amplitudes is proposed in present work. Firstly, the raw vibrational signal of fault bearing is decomposed into several SCs by performing Hankel matrix SVD, and each SC in time series format is obtained as well. Then, SES of each SC is obtained, as well as the corresponding kurtosis values. Furthermore, the maximum of the kurtosis values is picked out, and the ASC in accordance with the maximal kurtosis value can be regarded as the optimal one for further envelope analysis. Since SVD-KSES is mainly based on matrix calculation, it would be a time-saving approach which could provide timely detection of bearing failure. A numerical simulation of fault bearing vibration signal and public dataset from a test-to-failure experiment is adopted here to evaluate the efficiency of the proposed method.

Hereafter, this paper is organized as follows: introduction is given in the Section 1. Section 2 reviews the related theoretical basis. The SVD-KSES is illustrated in Section 3 along with its detailed process. Numerical simulation is conducted in Section 4, in which SVD-KSES is employed to a fault vibration signal with outer race defect. Following this, the experimental verification is carried out in Section 5. Finally, the conclusions are given in Section 6.

2. Review of the Theoretical Backgrounds

The acquired vibration signal can be regarded as a time series which cannot be fed into SVD directly. In present work, the Hankel matrix is applied to convert temporal vibration signal into matrix form.

2.1. Principal of SVD and Hankel Matrix Construction. Generally, the SVD is a linear algebra technique to achieve matrix transformation by which any given matrix $X(a \times b)$ can be decomposed into three matrices U, Σ, and V as equation (1), and its detailed forms are shown in equation (2).

$$X = U \sum V^T, \tag{1}$$

$$\begin{aligned} X = U \sum V^T &= [u_1, u_2, \ldots, u_b] \begin{bmatrix} \sigma_1 & 0 & \cdots & 0 \\ 0 & \sigma_2 & \ddots & \vdots \\ \vdots & \ddots & \ddots & 0 \\ 0 & \cdots & 0 & \sigma_b \end{bmatrix} \begin{bmatrix} v_1 \\ v_2 \\ \vdots \\ v_b \end{bmatrix} \\ &= \sum_{i=1}^{b} u_i \sigma_i v_i, \end{aligned} \tag{2}$$

where $U(a \times a)$ and $V(b \times b)$ are orthogonal matrices and Σ is a $(a \times b)$ diagonal matrix constituted of singular values $\sigma_1, \sigma_2, \sigma_3, \ldots, \sigma_b$ in decreasing order as equation (2) presents. The columns of the orthogonal matrix U are called the left singular vectors while the columns of the matrix V the right singular vectors. The left singular vectors of S are the eigenvectors of XX^T, and the right ones are the eigenvectors of X^TX. The principal of SVD noise elimination is to preserve the dominative SCs corresponding to the bigger SVs in the SVD partition of vibration signal based on the fact that white Gaussian has low cross correlation while fault-induced signal has high cross correlation.

Vibration signal should be firstly reshaped into a matrix as a preparation for SVD, and Hankel matrix is the one extensively used. Furthermore, Hankel-matrix-based SVD is widely used due to its zero-phase shift property and similar characteristics to wavelet transform, thus it is adopted here to achieve the pretreatment [25]. Given a measured signal $x = [x(1), x(2), \ldots, x(N)]$, its Hankel matrix can be rewritten as follows:

$$X = \begin{bmatrix} x(1) & x(2) & \cdots & x(b) \\ x(2) & x(3) & \cdots & x(b+1) \\ \vdots & \vdots & \ddots & \vdots \\ x(a) & x(a+1) & \cdots & x(N) \end{bmatrix}_{a \times b}, \quad (3)$$

where $a = N - b + 1$.

2.2. Squared Envelope Spectrum. Hilbert-transform-based envelope analysis is one of the widely used approaches to present the fault characteristic frequencies in bearing fault diagnosis. The envelope signal $E(t)$ of original signal $x(t)$ can be obtained by regarding the amplitude of the analytical signal derived from $x(t)$ as the real part and its Hilbert transform as the imaginary one. Performing the fast Fourier transform (FFT) of the envelope signal $E(t)$, the envelope spectrum can be obtained for further analysis.

Specifically, given a real signal $x(t)$, the Hilbert transform $h(t) = H\{x(t)\}$ is defined as follows [26]:

$$h(t) = H\{x(t)\} = \frac{1}{\pi} \int_{-\infty}^{\infty} \frac{x(\tau)}{t - \tau} d\tau = \frac{1}{\pi t} x(t), \quad (4)$$

where $h(t)$ is obtained from the convolution of the function $1/\pi t$ and the original signal $x(t)$. As the Fourier transform of $1/\pi t$ is

$$F\left(\frac{1}{\pi t}\right) = -j\mathrm{sgn}(f) = \begin{cases} -j, & \text{if } f > 0, \\ j, & \text{if } f < 0. \end{cases} \quad (5)$$

The Hilbert transform can be regarded as a filter of amplitude unity and phase $\pm 90^\circ$ depending on the sign of frequency of input signal spectrum. Then, the real signal $x(t)$ and its Hilbert transform $h(t)$ can constitute a new complex signal called the analytical signal shown in the following equation:

$$z(t) = x(t) + jh(t). \quad (6)$$

Moreover, envelope $E(t)$ of the complex signal $z(t)$ is defined as following:

$$E(t) = |z(t)| = |x(t) + jh(t)| = \sqrt{x^2(t) + h^2(t)}. \quad (7)$$

Until now, the envelope spectrum can be obtained by performing the FFT spectrum analysis of the envelope signal $E(t)$, from which some of the characteristic frequencies and their harmonics will clearly appear and those frequencies help to confirm bearing fault diagnosis.

The squared envelope (SE) is calculated as absolute squared value of the analytical signal which is obtained by Hilbert transform applied to the real signal $x(t)$. It is assumed that an instantaneous energy fluctuation would occur as a result of the corresponding transient impulses. While the SE signal can represent the instantaneous energy variation of vibration signal, it is reasonable to employ squared envelope to capture the instantaneous energy fluctuation [24]. Moreover, existing random or discrete noise components would hinder the envelope spectrum to present informative frequencies related to bearing failure, and squared envelope is an effective way to overcome this limitation [27]. Then, the SE of signal in equation (7) can be expressed as follows:

$$\mathrm{SE}(x(t)) = |E(x(t))|^2 = |x(t) + jh(t)|^2. \quad (8)$$

2.3. Kurtosis of the Squared Envelope Spectrum. Kurtosis has been proven to be a very useful monitoring parameter measuring the waveform peak and sensitive to the impulse characteristics of signal in rotating machinery fault diagnosis. Generally, kurtosis represents the characteristic of signals around its mean value and characterizes the strength of transient impulses [28] and is defined as the ratio of the fourth central moment of the signal to the squared second central moment of the signal [29], which is expressed in the following equation:

$$\mathrm{kurtosis}(x) = \frac{E\left\{(x - \mu)^4\right\}}{\sigma^4} - 3, \quad (9)$$

where σ and μ are the standard deviation and the mean of time series x, respectively, and $E\{\cdot\}$ is the expectation operator. The end of equation (9) "−3" is to make kurtosis of the normal distribution equal to zero. The essence of kurtosis is to indicate the peaks of the probability distribution associated to the instantaneous amplitude of the time series. To some extent, the frequency lines in SES have some similarities with temporal signal, and then kurtosis can extend its application into frequency domain and measure the information content of the envelope spectrum. Furthermore, the kurtosis of SES amplitudes outperforms kurtosis of temporal signal since the latter one is easily disturbed by noise and sensitive to random knocks [30].

3. The Flowchart of SVD-KSES Method

Based on the above introduction, the approach of the optimal SC selection for REB fault diagnosis based on SVD is described in this section, which is shown in Figure 1.

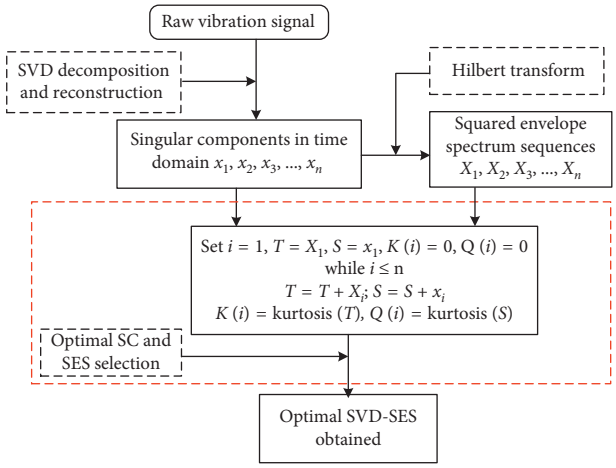

Figure 1: The SVD-KSES flowchart to select optimal SC.

Step 1. Signal decomposition and reconstruction by SVD.

The raw vibration signal is converted into the Hankel matrix on which SVD can be performed. Through the reverse Hankel matrix construction, several SCs in time series form can be obtained which are denoted as $x_1, x_2, \ldots, x_n$. These SCs are listed according to the SVs' descending order.

Step 2. Hilbert transform and squared envelope spectrum sequences.

With the Hilbert transform mentioned in Section 2.2, the squared envelope spectrum of each SC can be obtained, which is indicated by $X_1, X_2, \ldots, X_n$.

Step 3. Optimal SC selection and fault diagnosis of bearing.

As mentioned in Section 2, the SES provides the fault characteristic frequency along with its harmonics, and the kurtosis can reflect how much the potential the SES can convey the fault information. Therefore, kurtosis of the SES amplitudes is applied here to select the optimal SC, which is expected to provide more fault information about bearing state than other ones. Since origin signal can be recovered perfectly if all the SCs are added together, the effect of each single SC to accumulative SC should be evaluated quantitatively but less under study. Intuitionally, each single SC is added to accumulative SC (ASC) one by one, and kurtosis is introduced in this process to calculate its values of both the temporal SC and the SES of ASC when new SC is added. ASC is donated by S in Figure 1 and SES of ASC by T.

4. Numerical Simulation and Verification

To explain the procedure and efficiency of the SVD-KSES, a numeric simulation of fault bearing signal is conducted in this section. When rolling elements run over the defect area, such as the crack occurring on bearing component, a series of impulses will be generated and thus excite the resonance of the bearing or adjacent components at a certain rate which is called "bearing characteristic frequencies." The vital issue for bearing fault diagnosis is to detect these characteristic frequencies [31].

REB with fixed outer race is the common type used in practice and the so-called "bearing characteristic frequencies" vary according to the defect location (inner race, outer race, rolling element, and cage), the bearing structure parameters, and the machine shaft speed. According to the fault components of bearing, there are four characteristic frequencies, i.e., ball pass frequency of the outer race (BPFO), ball pass frequency of the inner race (BPFI), fundamental train frequency (FTF) related to cage speed rotation, and ball spin frequency (BSF). The following formulas represent these frequencies [32]:

$$\mathrm{BPFO} = \frac{z f_r}{2}\left(1 - \frac{d}{D}\cos\alpha\right), \tag{10}$$

$$\mathrm{BSF} = \frac{D}{2d}\left[1 - \left(\frac{d}{D}\right)^2 \cos^2\alpha\right], \tag{11}$$

$$\mathrm{FTF} = \frac{f_r}{2}\left(1 - \frac{d}{D}\cos\alpha\right), \tag{12}$$

$$\mathrm{BPFI} = \frac{z f_r}{2}\left(1 + \frac{d}{D}\cos\alpha\right), \tag{13}$$

where f_r is the rotating frequency of the shaft in Hz, d is the ball diameter, D is the pitch diameter, z is the number of rolling elements, and α is contact angle, respectively.

4.1. Numerical Signal. As aforementioned, defect rolling bearing under operation generates series of impulses in the vibration signal, and these impulses could excite the structure resonance between the defect zone and the accelerometers, thus leading to periodic impulses with damping oscillation waveform in the vibration signal [33]. The fault REB vibration signal is an amplitude modulation one where fault characteristic frequency is modulated to high resonance frequency band, and one fault model commonly used to simulate the fault REB vibration signal is expressed as follows:

$$x(t) = \sum_{i=1}^{M} A_i \cdot s\left(t - iT_0 - \tau_i\right) + n(t), \tag{14}$$

where $x(t)$ is the simulated fault vibration signal, $s(t)$ is the oscillating waveform, and $n(t)$ denotes the background noise. A_i is the amplitude modulator. M shows the number of simulated fault impulses. T_0 is the time period of impulses and τ_i is the period random fluctuation which indicates minor time slips of rolling elements. The oscillating waveform $s(t)$ can be indicated as

$$s(t) = e^{-Bt}\cos\left(2\pi f_n t + \varphi\right). \tag{15}$$

In equation (15), the oscillation waveform can be described as an exponential damping signal determined by parameter B and f_n. B is the damping coefficient related to the speed of oscillating decay and f_n is the oscillating

frequency reflecting the resonance information of the system. φ is the initial phase of the signal.

The amplitude modulator A_i determines the fault type of rolling bearings, and its mathematical expression can be expressed as follows:

$$A_i = A_0 \cos\left(2\pi f_m t + \varphi_A\right), \tag{16}$$

where A_0 is the amplitude constant which shows the maximum impulse amplitude when defect occurs in the rolling bearings. The defect location in rolling bearings determines the value of f_m, which can be replaced by characteristic frequencies [33]. Merging equations (14) and (15), the simulated signal can be written as

$$x(t) = \sum_{i=1}^{M} A_i \cdot e^{-Bt} \cos\left(2\pi f_n \left(t - iT_0 - \tau_i\right) + \varphi\right) + n(t). \tag{17}$$

For a brief and rational simulation, this part discusses the simulated vibration signal of REB with localized defect on outer race and signal accompanied by heavy noise as well. The sampling rate is 12 kHz and 2 kHz of resonant frequency. Additionally, the time length of the simulated signal is 0.68 s but only 0.4 s of the sampling time is presented in the following subsections for simplicity. The rotating speed of the bearing inner race keeps at 1772 rpm. Then, according to the structure parameters of 6205-2RS JEM SKF and fundamental fault frequency formula shown in equation (13), the fault characteristic frequency can be obtained whose value is 105.5 Hz. The last term in equation (17), $n(t)$, is referred to heavy Gaussian noise with SNR −14 dB. With these parameters mentioned above, the simulated periodic impulses and the vibration signal with background noise are shown in Figures 2(a) and 2(b), respectively. From Figure 2(b), it is apparent to see the fault-induced periodic impulses completely buried by the heavy background noise and barely noticeable. While frequency spectrums of both periodic impulses and mixed signal are depicted in Figure 2(c), the spectrum of fault vibration signal dotted by blue lines covers a wide frequency range, which seems like the one of Gaussian noise. Moreover, Figure 2(d) shows the corresponding squared envelope spectrums of the two signals, the period impulses and the mixed by heavy background noise, respectively. It is not easy to find the fault characteristic frequency or its harmonics. Then, a conclusion can be reached that the background noise is so strong that even the squared envelope spectrum provides little useful information concerning the fault. To a worse situation, the false frequency lines could emerge which would lead to wrong identification of faults.

4.2. Feasibility Illustration and Discussion. As mentioned in above parts, the core of the SVD-KSES is to find the maximal value of kurtosis of SES and subsequently the optimal SC for further analysis. For a brief description, the simulation fault signal colored by blue shown in Figure 2(b) is fed to the proposed method, and the kurtosis values of SES are plotted by black, as well as the kurtosis of the temporal SC by red color in Figure 3. From times of trial and by the principal of less amount of SC but maximal separation of vibration signal, 12 is set to the number of SC obtained by SVD process. Accordingly, there are 12 kurtosis values plotted in Figure 3, and the kurtosis of SES varies when the SCs are added together one by one, and the maximal value arises when the second SC is added. Moreover, since kurtosis is applied in time domain, the kurtosis values of each temporal SC are also plotted by red line and they manifest little change, which can be explained by the fact that the impulses carried by each SC are still buried by heavy noise even when they are decomposed by SVD. Therefore, the first two SCs are added together to represent the optimal one to form optimal SC for further analysis.

To evaluate the performance of proposed approach, the SES of the pure fault-induced impulses, the SES of optimal selected SC, and the SES of the mixed vibration signal are depicted in Figures 4(a)–4(c). The SES of pure impulses generated by fault in Figure 4(a) can provide the reference spectrum lines which help to confirm fault information of REB. Obviously, the optimal SES in Figure 4(b) provides clear spectrum lines, which is consistent with the corresponding line in Figure 4(a) and has more potential to make sure there are some defects or not of the REB than the one conveyed by SES in Figure 4(c). To highlight the SES with maximal kurtosis can be regarded as the optimal one, and the SES of the first 8 ASCs are plotted in Figure 5, from which the spectrum line to confirm the fault of REB colored by red is more apparent than others, which is consistent with the assumption in Figure 3. This demonstrates the practicability of the SVD-KSES again.

5. Experimental Verification

To investigate the efficiency of the proposed SVD-KSES for weak signal feature extraction, an experiment case collecting vibration signals of an early race defect from the natural degradation of a bearing is considered.

The vibration signals were collected by the NSF I/UCR Center for Intelligent Maintenance Systems (IMS), University of Cincinnati (Cincinnati, OH, USA) [34]. As shown in Figure 6, four test bearings (Rexnord ZA-2115) were installed on the shaft, each bearing was equipped by two PCB 353b33 ICP accelerometers from x and y directions, and the radial load of 2.7 kN was applied to the bearing 2 and 3. The shaft was driven by an AC motor through rub belts, and its speed was 2000 rpm. Eight vibration sensors could synchronously collect the vibration signal with a data acquisition of a National Instruments DAQ Card-6062E at sampling rate 20 kHz, and data length was 20480 points. A magnet was planted to collect the wearing or fault-induced debris in oil circulation. If the weight of the adhered debris or temperature exceeded a preset level, the test would be switched down automatically.

The structural parameters of tested bearing ZA-2115 and ball pass frequency outer (BPFO) of the tested bearing are listed in Table 1.

Kurtosis is employed here as a health indictor, and the kurtosis curve of the whole service life is presented in Figure 7, from which, the bearing running condition can be

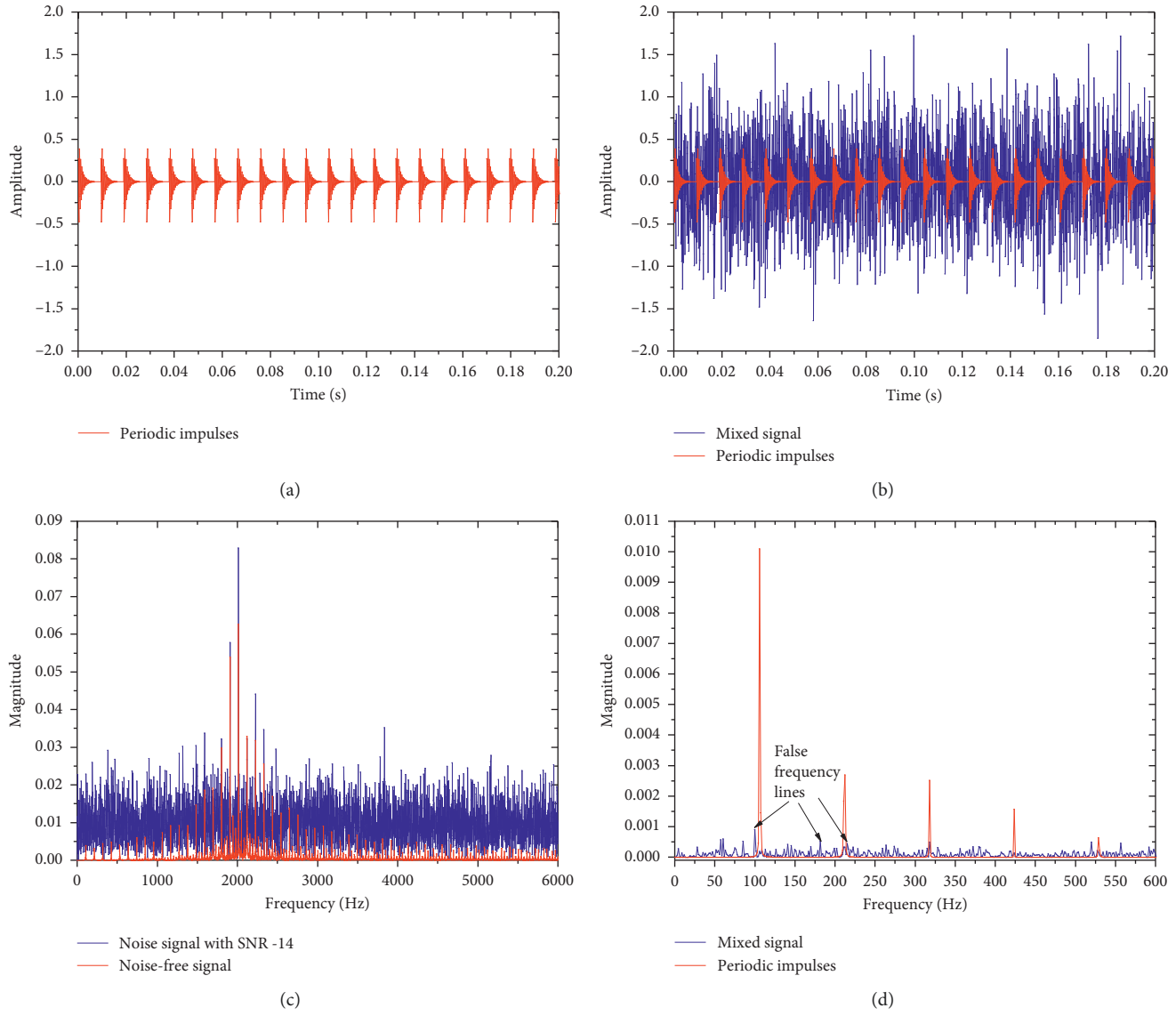

Figure 2: Simulation of the fault bearing vibration signal: (a) defect-induced periodic impulses; (b) the periodic impulses contaminated by noise; (c) frequency spectrums of pure periodic signal and noise-contained vibration signal; (d) squared envelope spectrums of the pure periodic signal and mixed signal.

divided into three stage. To make an apparent explanation, the reference line is also curved as a baseline which is calculated by the root mean square (RMS) of kurtosis values from the first 400 data points. Specifically, stage I covers near the half of the fault bearing life, and thus it can be regarded as normal operation period. Stage II lasts a relatively short time, and till the end of this stage, the kurtosis curve has a burst value, which can be regarded as a sign that the fault deteriorates obviously, and this stage should be accorded with fault degradation. In stage III, the kurtosis curves fluctuate and decline, but at the end of this stage, the kurtosis reaches a very high level, indicating the fault bearing stepping into a severe condition. In summary, the bearing in stage III is so extensively urgent that other mechanical components could suffer from abnormal or tempestuous vibration which may result in very worse situation any time, even unpredictable accidents and catastrophic failures. Consequently, stage II should be labeled as the early period of the fault development, and the end of this stage should be highly emphasized due to the burst in kurtosis curve. All in all, the in-time detection of REB fault can leave enough time to tackle the failure.

To verify the potential of SVD-KSES, stage II should be adopted here and is worth more investigation. The signal of the start and end point of this period is present in Figure 8, and from the Hilbert envelope spectrums shown in Figure 8, the fault characteristic frequency lines presented in Figure 8(b) are more evident than that in Figure 8(d) and so as to the waveforms in Figures 8(a) and 8(c), respectively. It is further demonstrated that the start of stage II can be taken as an incipient fault signal to validate the efficiency of SVD-KSES. Intuitively, the signal at point 535 should be considered more in later illustration.

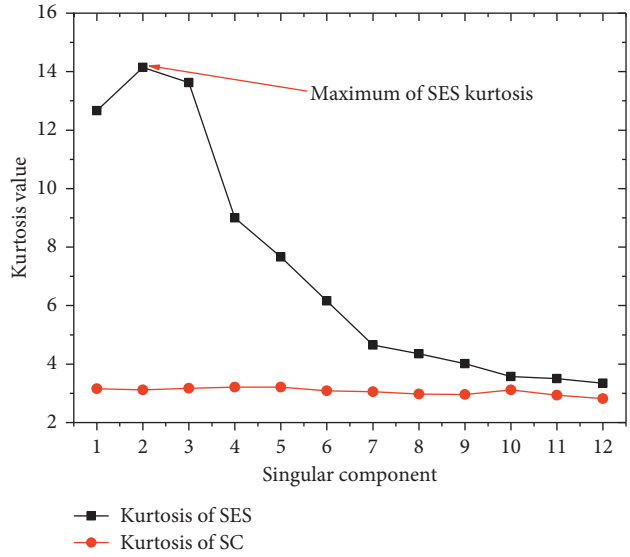

Figure 3: Kurtosis values of each SC and corresponding SES.

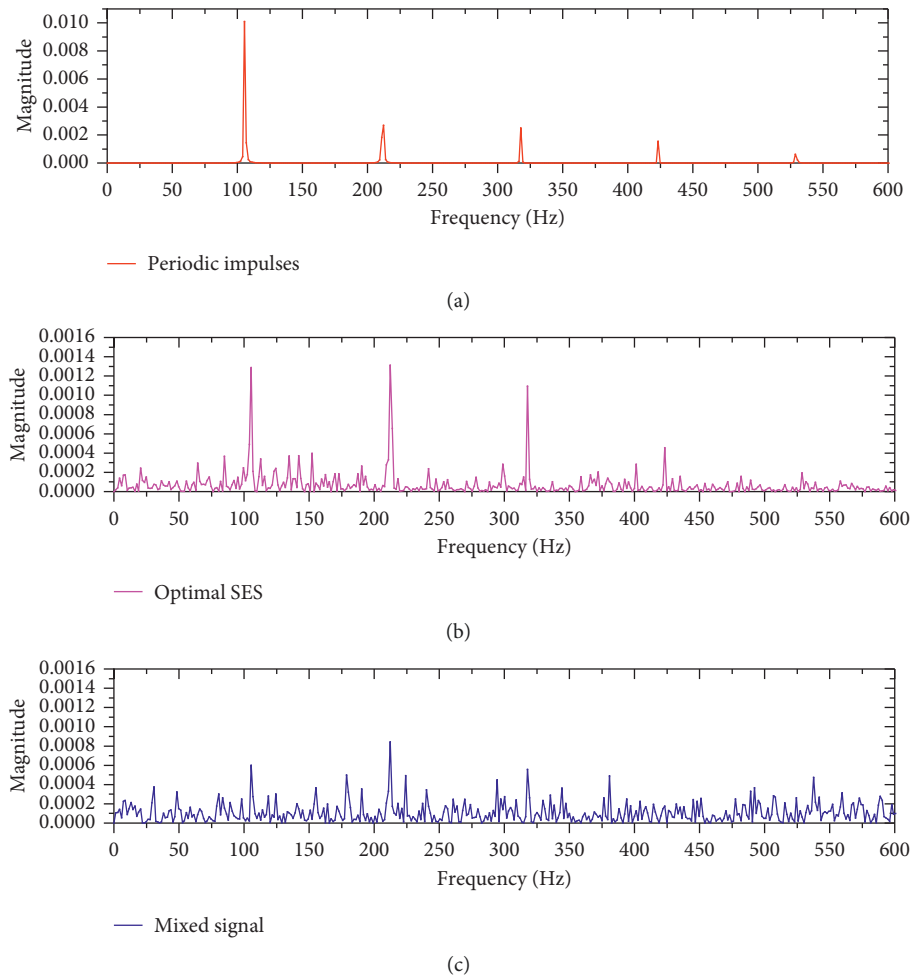

Figure 4: The results of mixed signal processed by SVD-KSES.

Performing the SVD-KSES on the vibration signal of point 535, the kurtosis values of SES from each ASC is curved in Figure 9. The peak arises when the second SC is added while the kurtosis of third SC waveform has a low value. According to the principle of SVD-KSES, the sum of first two SCs should give the optimal one on which the SES

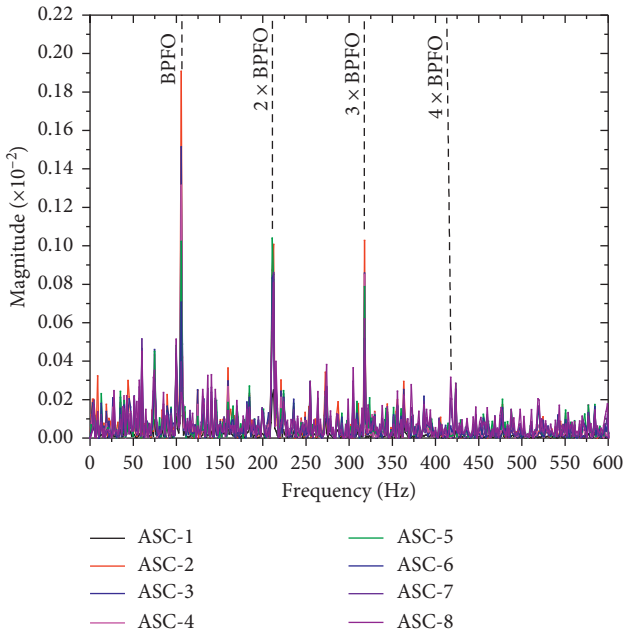

Figure 5: Squared envelope spectrums of partial ASCs.

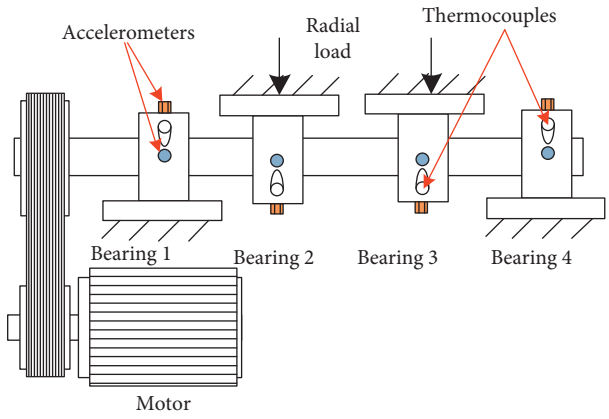

(a)

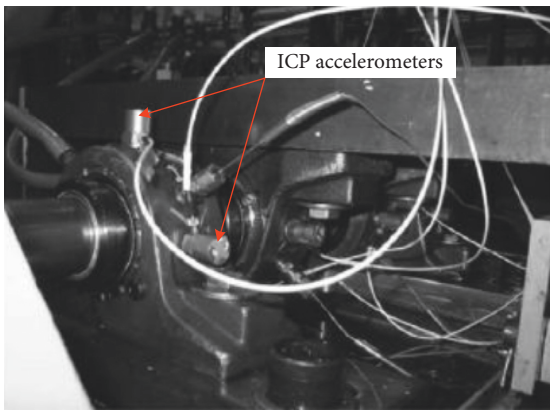

(b)

Figure 6: Bearing test rig and sensor placement illustration.

Table 1: Parameters of ZA-2115 and its fault frequency of outer race.

Item	Contact angle	Roller diameter	Pitch diameter	BPFO (Hz)
Value	15.17°	8.4 mm	71.5 mm	236.4

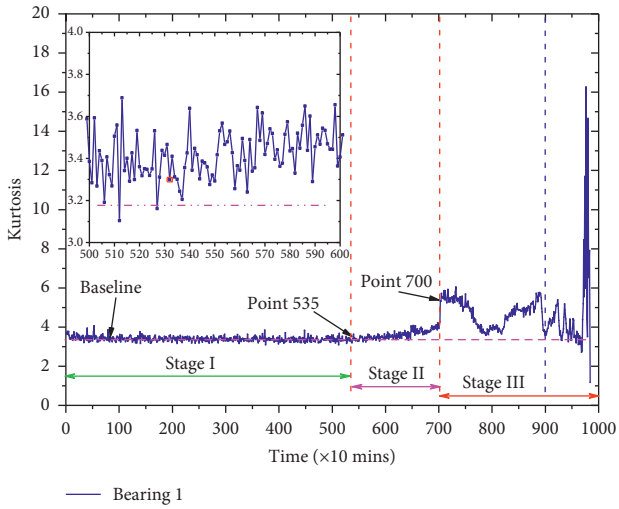

Figure 7: The kurtosis variation of bearing 1 during the experiment.

should be applied for fault diagnosis. The SESs of first 4 ASCs are shown in Figures 10(a)–10(d), respectively. The spectrum lines depicted in Figure 10(b) has relative higher magnitude and less noise compared with other ones, which demonstrates further that the second ASC is the optimal one, and the fault characteristic frequency lines are clearly observed to confirm the outer race fault.

To validate the SVD-KSES, conventional envelope spectrum is also conducted on the vibration signal in point 535, and the results are shown in Figure 11. Specifically, Figures 11(a) and 11(c) present the waveforms of vibration signal at point 535 and the optimal SC obtained by SVD-KSES, respectively; from the waveforms, nothing distinguishably different can be figured out by vision. The frequency lines, dotted by red and its two order and three order harmonics observed from Figure 11(d), are so apparent that it is enough to confirm the fault type of the bearing. To further illustrate the efficiency of SVD-KSES, the signal at point 535 is also fed to fast kurtogram [35] and paved in Figure 12, in which the optimal frequency band with maximal kurtosis value is indicated by the black rectangle. Then, the corresponding filtered signal is shown in Figure 11(e) and its SES in Figure 11(f) as well. The fast kurtogram method extracts the resonance frequency band but no obvious fault characteristic frequency modulation information can be observed in Figure 11(f) and thus leads to the inefficiency to detect bearing outer race fault. Contrastively, the same frequency lines are overwhelmed by unrelated spectrum lines or noise in Figure 11(f), which makes it less convincing to confirm whether there is a bearing fault existence or not than that in Figure 11(d). In

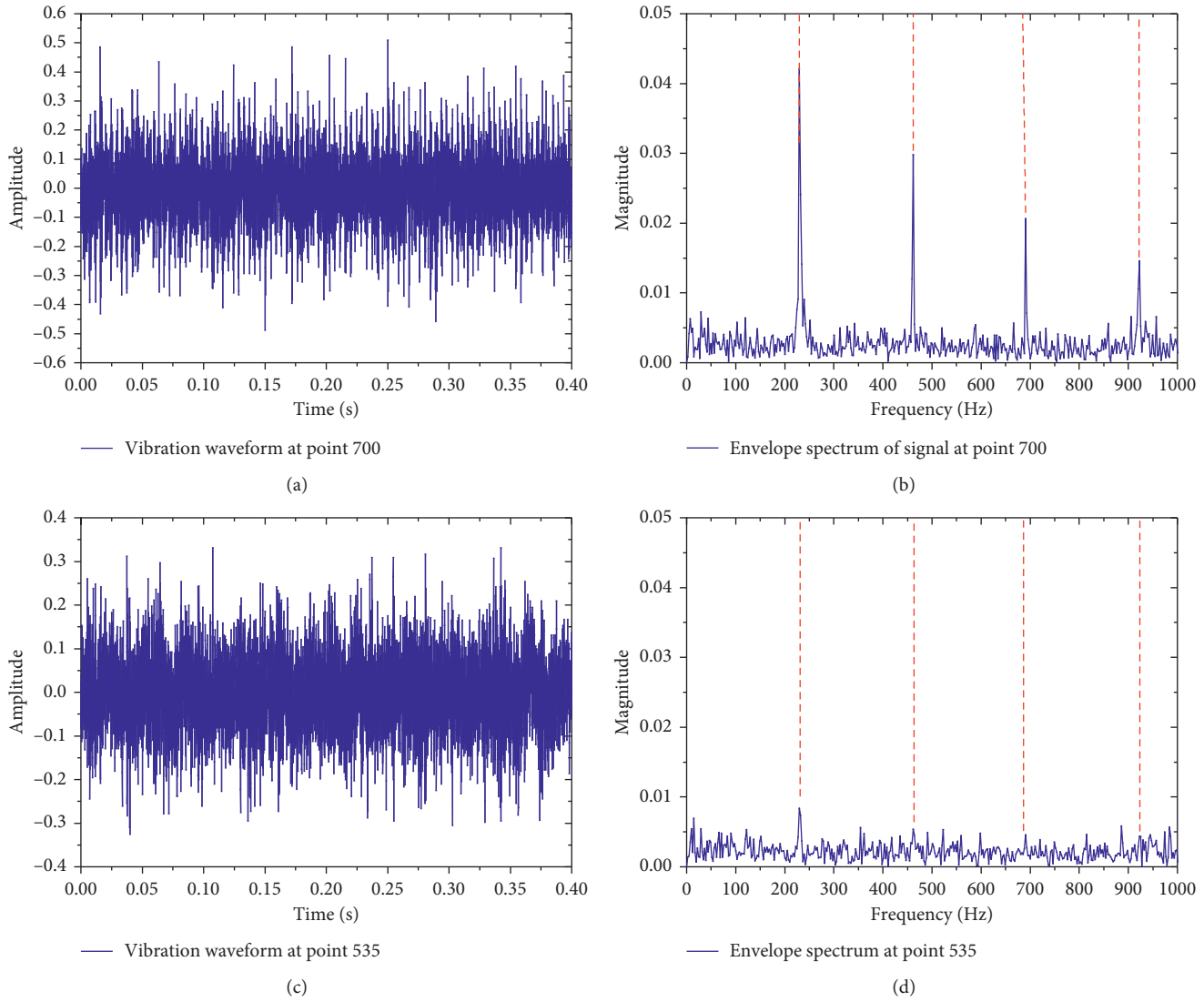

Figure 8: The start and end of stage II: (a) waveforms of signal at point 700; (b) envelope spectrum of signal at point 700; (c) waveforms of signal at point 535; (d) envelope spectrum of signal at point 535.

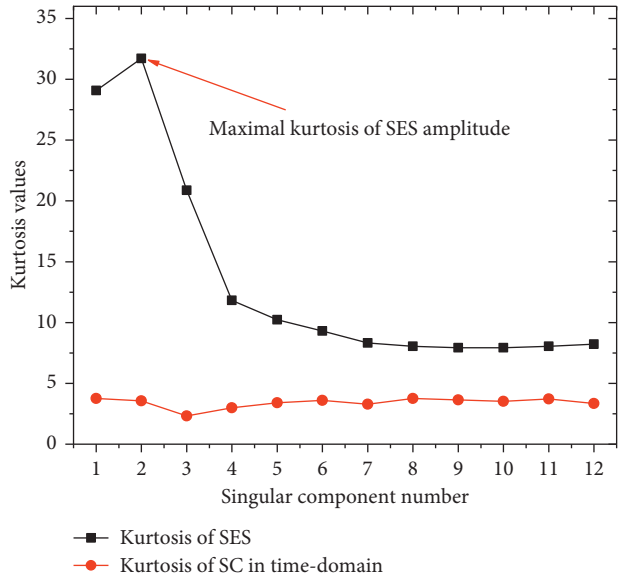

Figure 9: Kurtosis curves during SVD-KSES process.

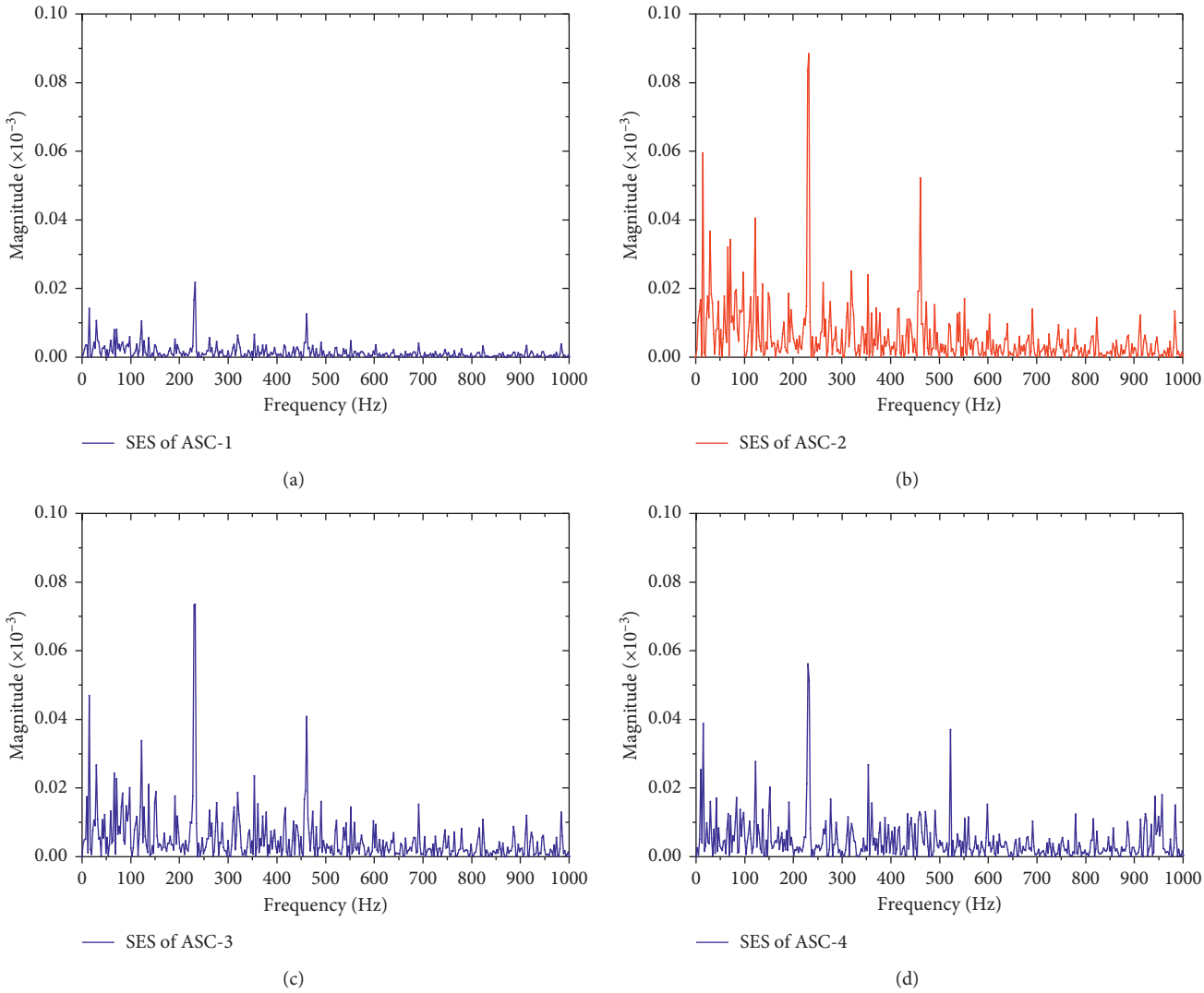

Figure 10: The squared envelope spectrums of first four ASCs: (a) the squared envelope spectrum of 1st ASC; (b) the squared envelope spectrum of 2nd ASC; (c) the squared envelope spectrum of 3rd ASC; (d) the squared envelope spectrum of 4th ASC.

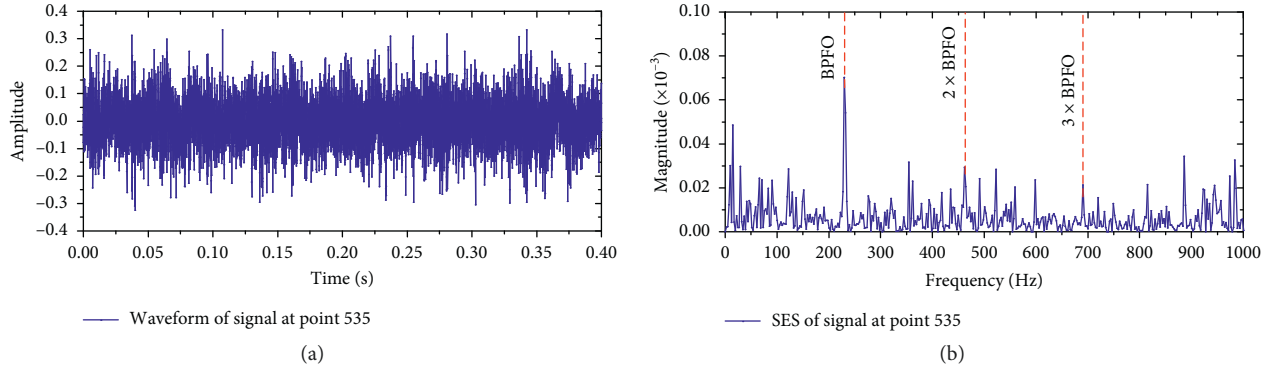

Figure 11: Continued.

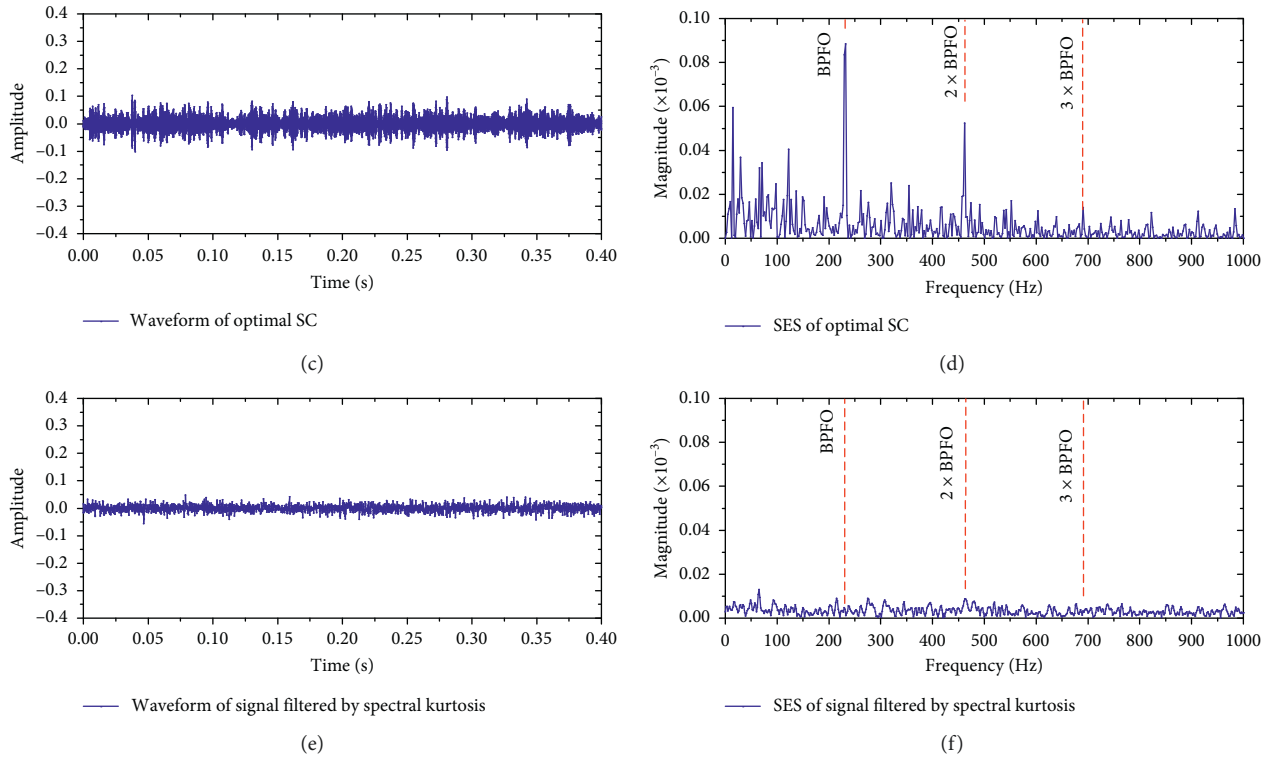

FIGURE 11: The results of the experiment: waveform at point 535 (a) and its squared envelope spectrum of incipient fault in point 535 (b); waveform of optimal SC (c) and its squared envelope spectrum (d); waveform of signal filtered by fast kurtogram (e) and its squared envelope spectrum (f).

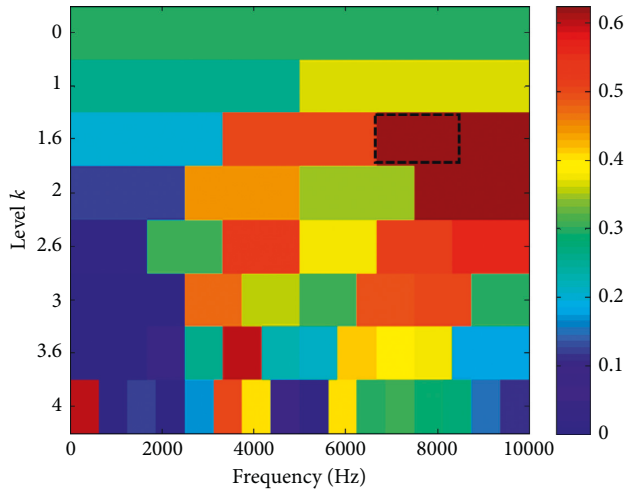

FIGURE 12: Fast kurtogram of signal at point 535.

conclusion, the analysis above demonstrates the efficiency of the proposed SVD-KESE in bearing fault diagnosis, particularly the incipient fault one.

6. Conclusions

This paper intends to exploit the combination of SVD and SES for the detection of bearing defects and the effect of each single SC to the accumulative SC. An indicator named KSES, whose definition is the kurtosis of squared envelope spectrum amplitudes, is applied here to weigh the informative potential of SCs obtained by performing SVD to vibration signal, thus sorting the most informative one to achieve bearing fault diagnosis. In selecting process, the ASC with the maximum of the KSES is taken as the most informative one and from which the bearing fault can be identified. The numerical simulation verifies the effectiveness of SVD-KSES, even in a heavy background

noise where SNR reaches −14 dB. Moreover, the bearing run-to-failure experiment is also considered, in which the fault bearing deteriorates naturally and the vibration signals are very close to real industrial application. The results of accelerating experiment confirm that the proposed SVD-KSES can detect the bearing outer race early at point 535, which is a common moment of incipient defect reported in a lot of journal articles about early fault diagnosis. The experimental data analysis results also verify SVD-KSES's efficiency in weak fault recognition.

Abbreviations

REB: Rolling element bearing
SVD: Singular value decomposition
SES: Squared envelope spectrum
KSES: Kurtosis of squared envelope spectrum
SC: Singular component
SV: Singular value
HHT: Hilbert-Huang transform
SSA: Singular spectrum analysis
QSSA: Quaternion singular spectrum analysis
SVR: Singular value ratio
FCF: Fault characteristic frequency
FFT: Fast Fourier transform
SE: Squared envelope
ASC: Accumulative singular component
BPFO: Ball pass frequency of outer race
BPFI: Ball pass frequency of inner race
FTF: Fundamental train frequency
BSF: Ball spin frequency
RMS: Root mean square.

Data Availability

All experiment data used during this research are openly available from the IMS Bearing Data deposited at https://doi.org/10.1016/j.jsv.2005.03.007. Specifically, the experiment data in our manuscript are downloaded from the IMS Bearing Data, which were generated by the NSF I/UCR Center for Intelligent Maintenance System with support from Rexnord Corp., Milwaukee, WI. In addition, the experiment data include three datasets, and the second one is employed in our study to verify our proposed method.

Conflicts of Interest

The authors declare that they have no conflicts of interest.

Acknowledgments

The authors are grateful to the Center of Intelligence Maintenance System (IMS), University of Cincinnati, for freely providing the experimental data. This work was supported by the National Natural Science Foundation (Grant no. 51175419) and Shaanxi Key Laboratory of Machinery Manufacturing Equipment Construction Project.

References

[1] A. Bellini, F. Filippetti, C. Tassoni, and G.-A. Capolino, "Advances in diagnostic techniques for induction machines," *IEEE Transactions on Industrial Electronics*, vol. 55, no. 12, pp. 4109–4126, 2008.

[2] S. Sheng, *Wind Turbine Gearbox Reliability Database, Condition Monitoring, and Operation and Maintenance Research Update*, National Renewable Energy Laboratory (NREL), Golden, CO, USA, 2016.

[3] Q. He, E. Wu, and Y. Pan, "Multi-scale stochastic resonance spectrogram for fault diagnosis of rolling element bearings," *Journal of Sound and Vibration*, vol. 420, pp. 174–184, 2018.

[4] A. Rai and S. H. Upadhyay, "A review on signal processing techniques utilized in the fault diagnosis of rolling element bearings," *Tribology International*, vol. 96, pp. 289–306, 2016.

[5] F. Cong, W. Zhong, S. Tong et al., "Research of singular value decomposition based on slip matrix for rolling bearing fault diagnosis," *Journal of Sound and Vibration*, vol. 344, pp. 447–463, 2015.

[6] V. C. M. N. Leite, J. G. B. da Silva, G. F. C. Veloso et al., "Detection of localized bearing faults in induction machines by spectral kurtosis and envelope analysis of stator current," *IEEE Transactions on Industrial Electronics*, vol. 62, no. 3, pp. 1855–1865, 2015.

[7] W. Guo, W. T. Peter, and A. Djordjevich, "Faulty bearing signal recovery from large noise using a hybrid method based on spectral kurtosis and ensemble empirical mode decomposition," *Measurement*, vol. 45, no. 5, pp. 1308–1322, 2012.

[8] Z. Huo, Y. Zhang, P. Francq et al., "Incipient fault diagnosis of roller bearing using optimized wavelet transform based multi-speed vibration signatures," *IEEE Access*, vol. 5, pp. 19442–19456, 2017.

[9] S. Mohanty, K. K. Gupta, and K. S. Raju, "Adaptive fault identification of bearing using empirical mode decomposition–principal component analysis-based average kurtosis technique," *IET Science, Measurement & Technology*, vol. 11, no. 1, pp. 30–40, 2017.

[10] H. Liu, X. Wang, and C. Lu, "Rolling bearing fault diagnosis under variable conditions using Hilbert-Huang transform and singular value decomposition," *Mathematical Problems in Engineering*, vol. 2014, Article ID 765621, 10 pages, 2014.

[11] M. Kang and J. M. Kim, "Singular value decomposition based feature extraction approaches for classifying faults of induction motors," *Mechanical Systems and Signal Processing*, vol. 41, no. 1-2, pp. 348–356, 2013.

[12] J. Gai and Y. Hu, "Research on fault diagnosis based on singular value decomposition and fuzzy neural network," *Shock and Vibration*, vol. 2018, Article ID 8218657, 7 pages, 2018.

[13] T. Liu, J. Chen, and G. Dong, "Singular spectrum analysis and continuous hidden Markov model for rolling element bearing fault diagnosis," *Journal of Vibration and Control*, vol. 21, no. 8, pp. 1506–1521, 2015.

[14] B. Kilundu, X. Chiementin, and P. Dehombreux, "Singular spectrum analysis for bearing defect detection," *Journal of Vibration and Acoustics*, vol. 133, no. 5, article 051007, 2011.

[15] B. Muruganatham, M. A. Sanjith, B. Krishnakumar et al., "Roller element bearing fault diagnosis using singular spectrum analysis," *Mechanical Systems and Signal Processing*, vol. 35, no. 1-2, pp. 150–166, 2013.

[16] C. Yi, Y. Lv, Z. Dang et al., "Quaternion singular spectrum analysis using convex optimization and its application to fault

diagnosis of rolling bearing," *Measurement*, vol. 103, pp. 321–332, 2017.

[17] F. Cong, J. Chen, G. Dong et al., "Short-time matrix series based singular value decomposition for rolling bearing fault diagnosis," *Mechanical Systems and Signal Processing*, vol. 34, no. 1-2, pp. 218–230, 2013.

[18] M. Zhao and X. Jia, "A novel strategy for signal denoising using reweighted SVD and its applications to weak fault feature enhancement of rotating machinery," *Mechanical Systems and Signal Processing*, vol. 94, pp. 129–147, 2017.

[19] S. Hussain and H. A. Gabbar, "Fault diagnosis in gearbox using adaptive wavelet filtering and shock response spectrum features extraction," *Structural Health Monitoring*, vol. 12, no. 2, pp. 169–180, 2013.

[20] L. Gelman, S. Kolbe, B. Shaw et al., "Novel adaptation of the spectral kurtosis for vibration diagnosis of gearboxes in non-stationary conditions," *Insight-Non-Destructive Testing and Condition Monitoring*, vol. 59, no. 8, pp. 434–439, 2017.

[21] T. Wang, F. Chu, Q. Han et al., "Compound faults detection in gearbox via meshing resonance and spectral kurtosis methods," *Journal of Sound and Vibration*, vol. 392, pp. 367–381, 2017.

[22] L. Wang, Z. Liu, Q. Miao et al., "Time–frequency analysis based on ensemble local mean decomposition and fast kurtogram for rotating machinery fault diagnosis," *Mechanical Systems and Signal Processing*, vol. 103, pp. 60–75, 2018.

[23] T. Barszcz and A. JabŁoński, "A novel method for the optimal band selection for vibration signal demodulation and comparison with the Kurtogram," *Mechanical Systems and Signal Processing*, vol. 25, no. 1, pp. 431–451, 2011.

[24] J. Antoni, "The infogram: entropic evidence of the signature of repetitive transients," *Mechanical Systems and Signal Processing*, vol. 74, pp. 73–94, 2016.

[25] H. Jiang, J. Chen, G. Dong et al., "Study on Hankel matrix-based SVD and its application in rolling element bearing fault diagnosis," *Mechanical Systems and Signal Processing*, vol. 52-53, pp. 338–359, 2015.

[26] B. Boashash, "Estimating and interpreting the instantaneous frequency of a signal. II. Algorithms and applications," *Proceedings of the IEEE*, vol. 80, no. 4, pp. 540–568, 1992.

[27] V. C. M. N. Leite, J. G. B. da Silva, G. L. Torres et al., "Bearing fault detection in induction machine using squared envelope analysis of stator current," in *Bearing Technology*, InTech, London, UK, 2017.

[28] X. Chen, B. Zhang, F. Feng et al., "Optimal resonant band demodulation based on an improved correlated kurtosis and its application in bearing fault diagnosis," *Sensors*, vol. 17, no. 2, p. 360, 2017.

[29] Y. Wang, J. Xiang, R. Markert et al., "Spectral kurtosis for fault detection, diagnosis and prognostics of rotating machines: a review with applications," *Mechanical Systems and Signal Processing*, vol. 66, pp. 679–698, 2016.

[30] S. Wan, X. Zhang, and L. Dou, "Shannon entropy of binary wavelet packet subbands and its application in bearing fault extraction," *Entropy*, vol. 20, no. 5, p. 388, 2018.

[31] J. Duan, T. Shi, H. Zhou et al., "Multiband envelope spectra extraction for fault diagnosis of rolling element bearings," *Sensors*, vol. 18, no. 5, p. 1466, 2018.

[32] R. B. Randall and J. Antoni, "Rolling element bearing diagnostics—a tutorial," *Mechanical Systems and Signal Processing*, vol. 25, no. 2, pp. 485–520, 2011.

[33] F. Cong, J. Chen, and G. Dong, "Research on the order selection of the autoregressive modelling for rolling bearing diagnosis," *Proceedings of the Institution of Mechanical Engineers, Part C: Journal of Mechanical Engineering Science*, vol. 224, no. 10, pp. 2289–2297, 2010.

[34] H. Qiu, J. Lee, J. Lin et al., "Wavelet filter-based weak signature detection method and its application on rolling element bearing prognostics," *Journal of Sound and Vibration*, vol. 289, no. 4-5, pp. 1066–1090, 2006.

[35] J. Antoni, "Fast computation of the kurtogram for the detection of transient faults," *Mechanical Systems and Signal Processing*, vol. 21, no. 1, pp. 108–124, 2007.